Phase Field/Fluctuating Hydrodynamics approach for bubble nucleation

[1]Mirko Gallo; [1]Francesco Magaletti; [1] Carlo Massimo Casciola*

[1]Dept. of Mechanical and Aerospace Engineering, Sapienza University of Rome, Roma, Italy

Abstract

Vapour bubbles form in liquids by two main mechanisms: boiling, by increasing the temperature over the boiling threshold, and cavitation, by reducing the pressure below the vapour pressure threshold. The liquid can be held in these metastable states (overheating and tensile conditions, respectively) for a long time without forming bubbles. Bubble nucleation is indeed an activated process, requiring a significant amount of energy to overcome the free energy barrier and bring the liquid from the metastable conditions to the thermodynamically stable state where vapour is observed. Nowadays molecular dynamics is the unique tool to investigate such thermally activated processes. However, its computational cost limits its application to small systems (less than few tenth of nanometers) and to very short times, preventing the study of hydrodynamic interactions. In this work a continuum diffuse interface model of the two-phase fluid has been embedded with thermal fluctuations in the context of the so-called Fluctuating Hydrodynamics (FH), enabling the description of the liquid-vapour transition in extended systems and the evaluation of bubble nucleation rates in different metastable conditions by means of numerical simulations. Such an approach is expected to have a huge impact on the understanding of the nucleation dynamics since, by reducing the computational cost by orders of magnitude, it allows the unique possibility of investigating systems of realistic dimensions on macroscopic time scales.

Keywords: boiling; cavitation; diffuse interface; fluctuating hydrodynamics; thermal fluctuations

Introduction

Thermal fluctuations play a dominant role in mesoscopic phenomena occurring in fluids. Since the pioneering work of Landau and Lifshitz in the late fifties [1], several models have been developed [2] to properly include stochastic terms in the governing equations contributing to the growing field of ‘‘Fluctuating Hydrodynamics’’ (FH). Also motivated by applications, these efforts were followed by the exponential increase of specialised numerical methods for stochastic differential equations [3-5]. Fluctuations are crucial in a number of contexts, e.g., among others, flow-driven micro-devices, biological and lipid membranes [6], systems exploiting ratchet motion [7] like Brownian engines and artificial molecular motors [8, 9]. Presumably, nucleation - the precursor of the phase change in metastable systems - is however the most common fluctuation-dominated phenomenology found in applications. Examples are cavitation [10], freezing rain [11], or the intrusion of liquids in microporous materials [12], to cite a few. Since the energy barriers for phase transition is overcome by thermal fluctuations [13-17], the nucleation time may be long and the phenomenon is labeled as a ‘‘rare event’’. Such problems are typically addressed by molecular dynamics (MD) simulations [18] which, for their computational cost, are limited to systems too small to rise a direct technological interest.

Here homogeneous vapour bubble nucleation in a metastable liquid is addressed through a novel approach based on a diffuse interface description [19] of the two-phase system embedded with thermal fluctuations [20] that can describe both the thermodynamic and the fluid dynamics fields [21, 22], see [23] for applications to the spinodal decomposition in a liquid--vapour system.

Mathematical model

The model is based on the Van der Waals’s square gradient approximation [19] of the Helmholtz free energy

$$F\left[\rho,\theta\right]=\int_{V} dV\left(f_0\left(\rho,\theta\right)+\frac{1}{2}\lambda\nabla\rho\cdot\nabla\rho\right), \qquad (1)$$

*Corresponding Author, Carlo Massimo Casciola: carlomassimo.casciola@uniroma1.it

where f_0 is the classical bulk term, function of density ρ and temperature θ, and λ is related to the (equilibrium) surface tension γ and interface thickness [1,2].

The (fluctuating) hydrodynamic fields are governed by mass, momentum and energy conservation, with the addition of stochastic contributions:

$$\frac{\partial \rho}{\partial t} + \nabla \cdot \left(\rho \mathbf{u}\right) = 0\,,$$

$$\frac{\partial \rho \mathbf{u}}{\partial t} + \nabla \cdot \left(\rho \mathbf{u} \otimes \mathbf{u}\right) = -\nabla p + \nabla \cdot \boldsymbol{\Sigma} + \nabla \cdot \boldsymbol{\delta \Sigma}\,,$$

$$\frac{\partial E}{\partial t} + \nabla \cdot (\mathbf{u} E) = \nabla \cdot \left(-p\,\mathbf{u} + \mathbf{u} \cdot \boldsymbol{\Sigma} - \mathbf{q}\right) + + \nabla \cdot \left(\mathbf{u} \cdot \boldsymbol{\delta \Sigma} - \boldsymbol{\delta q}\right)\,,$$

where $\mathbf{u}$ is the fluid velocity, $p = \rho^2 \partial (f_0/\rho)/\partial \rho$ the pressure and $E = \mathscr{U} + 1/2\rho\,|\mathbf{u}|^2 + 1/2\lambda\,|\nabla \rho\,|^2$ the energy density, with $\mathscr{U}$ the internal energy per unit volume. $\boldsymbol{\Sigma}$ and $\mathbf{q}$ are the deterministic stress tensor and energy flux, respectively. The prefix δ denotes the stochastic contributions, which statistical properties follow by enforcing the *fluctuation-dissipation balance* (FDB):

$$\left\langle \boldsymbol{\delta \Sigma}(\hat{x}, \hat{t}\,) \otimes \boldsymbol{\delta \Sigma}^{\dagger}(\tilde{x}, \tilde{t}\,) \right\rangle = 2 \mathrm{k}_B \theta \mu \left(\delta_{\alpha\nu}\delta_{\beta\eta} + \delta_{\alpha\eta}\delta_{\beta\nu} - 2/3 \delta_{\alpha\beta}\delta_{\nu\eta}\right) \delta(\hat{x} - \tilde{x}) \delta(\hat{t} - \tilde{t}\,),$$

$$\left\langle \boldsymbol{\delta q}(\hat{x}, \hat{t}\,) \otimes \boldsymbol{\delta q}^{\dagger}(\tilde{x}, \tilde{t}\,) \right\rangle = 2 \mathrm{k}_B \theta^2 k\, \delta_{\alpha\beta} \delta(\hat{x} - \tilde{x}) \delta(\hat{t} - \tilde{t}\,),$$

with μ and k the dynamic viscosity and the thermal conductivity, respectively. The cross-correlation between tensors of different rank vanishes due to the Curie-Prigogine principle, $\left\langle \delta \mathbf{q}^{\dagger}(\tilde{x}, \tilde{t}\,) \otimes \delta \boldsymbol{\Sigma}(\hat{x}, \hat{t}\,) \right\rangle = 0$. $\boldsymbol{\Sigma}$ and $\boldsymbol{q}$ follow from standard non-equilibrium thermodynamics considerations [1,2] as

$$\boldsymbol{\Sigma} = \left(\frac{\lambda}{2} |\nabla \rho\,|^2 + \rho \nabla \cdot \left(\lambda \nabla \rho\right)\right) \boldsymbol{I} - \lambda \nabla \rho \otimes \nabla \rho + + \mu \left[\left(\nabla \mathbf{u} + \nabla \mathbf{u}^T\right) - \frac{2}{3} \nabla \cdot \mathbf{u} \boldsymbol{I}\right],$$
$$\boldsymbol{q} = \lambda \rho \nabla \rho \nabla \cdot \mathbf{u} - k \nabla \theta\,.$$

Bubble-Nucleation Simulations

Homogeneous vapour bubble nucleation in a metastable liquid enclosed in a cubic box with periodic boundary conditions is studied by numerically solving the equations presented in the previous section. The equation of state corresponds to a Lennard-Jones fluid [24] to allow comparison with available MD results. The system volume $V^* = (600)^3$ is discretised on a uniform grid with 50 cells per direction and several metastable conditions are investigated. Here we report the *long-time dynamics* evolving from the metastable thermodynamic condition $\theta = 1.25\,\rho_L = 0.46$ where strong hydrodynamic interactions, e.g., bubble collapse, coalescence and expansion, take place during nucleation. A few snapshots of the system evolution in the different metastable conditions are shown in the left panels of Fig. 1. Starting from the homogeneous liquid, fluctuations lead the system to nucleate the vapour phase. The initial shape of the nuclei is far from spherical, as observed in MD [18]. After reaching the critical size, the bubbles start expanding and the system stabilises in a state characterised by several vapour bubbles in equilibrium with the surrounding liquid. Bubble number and dimensions is dictated by the initial metastable condition. FH provides access the bubbles long-time dynamics in a very large system, taking in full account their hydrodynamic interactions. Before addressing the nucleation dynamics in detail, it is worth introducing the notion of critical bubble, in order to be able to identify the genuinely nucleated bubbles and their long term evolution.

The critical bubble

*Corresponding Author, Carlo Massimo Casciola: carlomassimo.casciola@uniroma1.it

It is known that bubbles smaller than critical shrink and disappear, while supercritical one may grow to macroscopic size. The demarcation line is the critical bubble which may be determined from the Helmholtz free energy, eq. (1). Minimising F identifies the critical state where the generalised chemical potential $\mu_c = \mu_c^b(\rho) - \lambda \nabla^2 \rho$ equals the external chemical potential μ_{eq}. The critical density profile under spherical symmetry can be found by the string method proposed in [25], see also [26], which identifies both the critical nucleus and the transition path joining the metastable liquid condition to the cavitated state. The method consists in initialising a set of N_s density fields $\{\rho^k(r)\}$, $k = 1,\ldots, N_s$, the so-called *string,* joining the metastable liquid state and the critical state. The head of the string is the uniform density of the liquid $\rho^1(r) = \rho_L$; the tail, $\rho^{N_s}(r)$, is initialised as a tanh profile approximating the critical nucleus which is obtained from classical nucleation theory (CNT) [27]; the intermediate fields are initialised by interpolation of these two density profiles, $\rho^k(r) = (1 - k/N_s)\rho^1(r) + k/N_s \rho^{N_s}(r)$. The string algorithm involves two steps. 1) All the images $\rho^k(r)$ are evolved over one pseudo-time step $\Delta\tau$ following the steepest-descent algorithm consisting in evolving the following relaxation dynamics in the pseudo-time

$$\frac{\partial \rho}{\partial \tau} = \mu_{eq} - \left[\mu_c^b(\rho) - \frac{\lambda}{r^2} \frac{\partial}{\partial r} \left(r^2 \frac{\partial \rho}{\partial r} \right) \right] .$$

Special attention is dedicated to the tail of the string that needs to climb the energy landscape up to the saddle point. An extra driving force, directed in the direction tangential to the string at the tail, is applied to allow the climbing motion. 2) The images are redistributed along the string following a re-parameterisation procedure by equal arc length. The algorithm is arrested when the string converges within a prescribed tolerance thereby identifying the transition path as the sequence of density fields along the string. Critical radius and free energy barrier $R_c = \int_0^\infty r(\partial \rho_c/\partial r)^2 r^2 \, \mathrm{d}r / \int_0^\infty (\partial \rho_c/\partial r) r^2 \, \mathrm{d}r$ [28] and $\widetilde{\Delta\Omega} = \int_0^\infty \left[w(\rho_c(r)) - w(\rho_L) \right] 4\pi r^2 \mathrm{d}r$, respectively, follow from the critical density profile $\rho_c(r)$. In the following sections the critical bubble, and its size in particular, will be used to discriminate whether the bubbles found in the FH simulations to be discussed are sub- or supercritical, thus allowing to evaluate the nucleation rate as the number of supercritical bubbles formed per unit volume and time.

Bubble Kinematics

In order to extract the bubble kinematics and track bubble motions, the evolution of the density iso-surface $\rho[(\mathbf{x}(\eta, t), t)] = \rho_0$, representing the nominal interface represented as $\mathbf{x} = \mathbf{x}\left(\eta, t\right)$, is considered. Its time derivative $d\rho[(\mathbf{x}\left(\eta, t\right), t)]/dt = \partial\rho/\partial t + \dot{\mathbf{x}} \cdot \nabla\rho = 0$ defines the interface velocity $\mathbf{w}(\mathbf{x}, t) := \dot{\mathbf{x}} = -\partial\rho/\partial t \, \nabla\rho / |\nabla\rho|^2$. Hence the evolution of a generic physical quantity $\phi(\mathbf{x}, t)$ related the bubble B_i is given by

$$\dot{\Phi} = \frac{d}{dt} \int_{\mathbf{B}_i(t)} \phi(\mathbf{x}, t) \, dV = \frac{d}{dt} \int_{\mathbf{B}_i^\eta} \phi\left(\mathbf{x}\left(\eta, t\right), t\right) \mathbf{J}^\eta \, dV^\eta = \int_{\mathbf{B}_i(t)} \frac{D^{(w)}}{Dt} \phi + \phi \nabla \cdot \mathbf{w} \, dV, \qquad (2)$$

where $D^{(w)}/Dt = \partial/\partial t + \mathbf{w} \cdot \nabla$ is the total derivative following the $\mathbf{w}$ velocity field and $\mathbf{J}^\eta = |\partial \mathbf{x}/\partial \eta|$ is the Jacobian determinant, with derivative $\dot{\mathbf{J}}^\eta = \mathbf{J}^\eta \nabla \cdot \mathbf{w}$. Defined the peculiar velocity $\mathbf{w}_i'(\mathbf{x}, t) := \mathbf{w}_i(\mathbf{x}, t) - \mathbf{u}(\mathbf{x}, t)$ and making use of eq. (2) with $\phi(\mathbf{x}, t) = \rho(\mathbf{x}, t)$ combined with mass conservation $\partial\rho/\partial t + \nabla \cdot \left(\rho \mathbf{u}\right) = 0$, the bubble mass is found to obey

$$\dot{M}_{B_i} = \frac{d}{dt} \int_{\mathbf{B}_i(t)} \rho(\mathbf{x}, t) \, dV = \oint_{\partial \mathbf{B}_i(t)} \rho(\mathbf{x}, t) \, \mathbf{w}_i'(\mathbf{x}, t) \cdot \mathbf{n} \, dS,$$

with $\mathbf{B_i(t)}$ the bubble domain. The bubble centre of mass velocity is then

$$\dot{\mathbf{X}}_{g_i} = \frac{1}{M_{B_i}} \frac{d}{dt} \int_{\mathbf{B_i(t)}} \mathbf{x} \rho(\mathbf{x}, t) \, dV - \frac{\dot{M}_{B_i}}{M_{B_i}} \mathbf{X}_{g_i} = \frac{1}{M_{B_i}} \int_{\mathbf{B_i(t)}} \rho(\mathbf{x}, t) \, \mathbf{u}(\mathbf{x}, t) - \nabla \cdot \mathbf{G}_i \left(\mathbf{x}, t, \mathbf{X}_{g_i}\right) dV,$$

*Corresponding Author, Carlo Massimo Casciola: carlomassimo.casciola@uniroma1.it

where $\mathbf{G}_i\left(\mathbf{x},t,\mathbf{X}_{g_i}\right)=\rho\left(\mathbf{x},t\right)\left(\mathbf{x}-\mathbf{X}_{g_i}\right)\otimes\left(\partial\rho/\partial t\,\nabla\rho/|\nabla|^2-\mathbf{u}\left(\mathbf{x},t\right)\right)$. Similarly the time derivative of the bubble volumes reads $\dot{V}_{B_i}=\oint_{\partial\mathbf{B_i(t)}}\mathbf{w}_i^{'}\left(\mathbf{x},t\right)\cdot\mathbf{n}\,dS$.

On the basis of the above analysis, an algorithm can be implemented to identify and track the distinct bubbles and their properties. First, a *cell-flagging* procedure based on the local density is used to identify the grid cells considered as non-liquid (cut-off density $\rho_{cut}=\rho_c(R_c)$, corresponding to the critical density at the nominal radius of the critical bubble). A clustering technique based on a region growing procedure is then applied to the non-liquid cells to determine when a neighbouring cell should be added to the current cluster. The process is iterated until all the detected vapour (non-liquid) cells has been clustered into distinct bubbles. The volume of the *k*-th bubble is used as the order parameter to identify the supercritical bubbles defined as those which volume exceeds the critical volume. For each bubble present in the field, this procedure allows to obtain mass centre trajectory and volume evolution and to identify the coalescence events, see the left panel of Fig. 1.

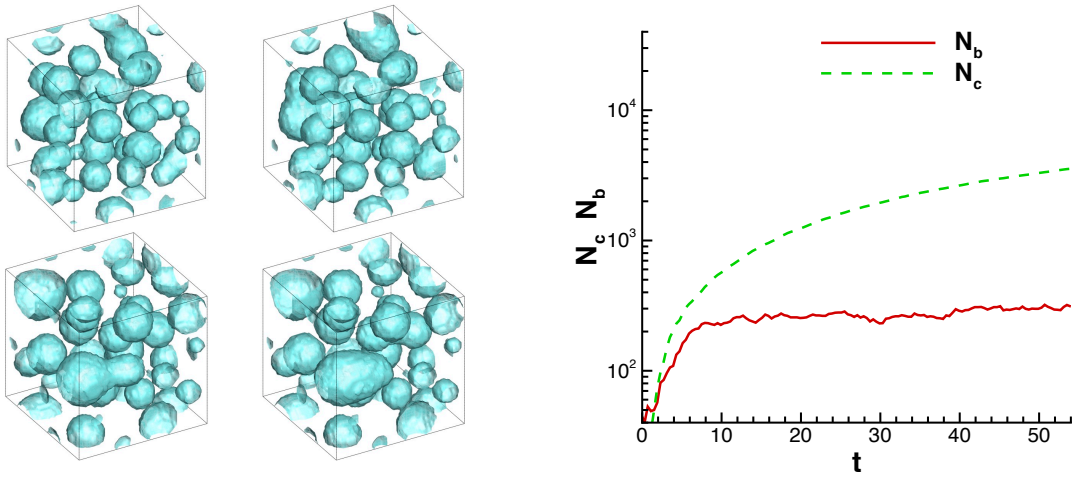

Figure 1. Left panel: snapshots of bubble configurations during the nucleation process to highlight the coalescence process. Right panel: Time evolution of the number of supercritical bubbles and the total collapsed supercritical bubble up to time instant t.

The central observable is the nucleation rate J, defined as the number of supercritical bubbles formed per unit volume and time. CNT [27] provides an estimate of the energy barrier $\widetilde{\Delta\Omega}_{CNT}$ and consequently of the nucleation rate as $J_{CNT}=n_L\sqrt{2\gamma/m\pi}\exp(-\widetilde{\Delta\Omega}_{CNT}/k_B\theta)$, where n_L is the liquid number density. CNT can be compared with the nucleation rate J_{FH} from FH simulations, estimated as the slope of the linear initial part of the curve giving the number of supercritical bubbles N_b vs time in the right panel of Fig. 1.

Discussion of the results

As known from the literature, CNT over-estimates the energy barrier near the spinodal condition and tends to behave better at lower metastabilities. Consistently the barrier obtained from the string method are smaller than CNT ones, Table 1. Notwithstanding this point the rates, J, evaluated with CNT are puzzlingly larger than those from FH. In order to correctly understand this point, it is crucial to take into account the confinement affecting a constant mass/ constant volume system. In these conditions, the larger the number of nucleated bubbles the more the liquid is compressed. As a result the nucleation process is discouraged and consequently the nucleation rate is reduced, thus explaining the lower nucleation rate of FH with respect to CNT. In fact, by tracking all the vapour clusters in the system during the initial nucleation stage (characterised by constant rate) we observed that the number of collapsed bubbles after crossing the critical size is of the same order of (and often greater than) the number of the "survived" ones. In fact, if all the bubbles survived we would have obtained a rate larger than predicted by CNT, consistently with the reduced free energy barrier. This point is illustrated in the right part of Fig. 1 where the evolution of the number of supercritical bubbles N_b and of the number of supercritical bubbles N_c collapsed up to current time is

*Corresponding Author, Carlo Massimo Casciola: carlomassimo.casciola@uniroma1.it

$\widetilde{\Delta\Omega}/\theta_0$	$\widetilde{\Delta\Omega}_{CNT}/\theta_0$	J_{FH}	J_{CNT}	J_{FH}^{tot}
5.90	14.05	$1.3 \cdot 10^{-8}$	$7.0 \cdot 10^{-8}$	$3.2 \cdot 10^{-7}$

Table 1. Comparison between CNT and FH rate, the free energy barrier for bubble nucleation from the liquid is evaluated with the string method.

shown. In absence of collapses, the total number of bubbles in the system would have been $N_{tot} = N_b + N_c$ and the rate would have been larger by roughly a factor 10^2, consistently with the lower free energy barriers reported in Table 1.

Conclusion

In conclusion, we have shown that a Van der Walls/Navier-Stokes/Landau-Lifshitz model can properly capture the vapour bubble nucleation process. The model works equally well in the context of cavitation, where nucleation is induced by pressure decrease, and boiling, where the phase transition is due to increased temperature. Both processes involve significant metastabilities. The continuum description of the two phase system endowed with proper thermal fluctuations satisfying the appropriate form of fluctuation dissipation balance is able to describe the thermally activated transition process and predict the nucleation rate. Unique feature of the model is the ability to deal with extended systems, under non-equilibrium and unsteady conditions like those most often encountered in applications involving liquid-vapour phase transition. Particularly significant is the interaction of the microscopic process of nucleation with the hydrodynamic scales that couples in both directions the phase transition to the macroscopic flow.

Acknowledgments

The research leading to these results has received funding from the European Research Council under the European Union's Seventh Framework Programme (FP7/ 2007-2013)/ERC Grant agreement no. [339446].

References

1. Landau, L. and E. Lifshitz, *Statistical physics, vol. 5.* Course of theoretical physics, 1980. **30**.
2. Fox, R.F. and G.E. Uhlenbeck, Contributions to Non−Equilibrium Thermodynamics. I. Theory of Hydrodynamical Fluctuations. The Physics of Fluids, 1970. **13**(8): p. 1893-1902.
3. Donev, A., et al., *On the accuracy of finite-volume schemes for fluctuating hydrodynamics.* Communications in Applied Mathematics and Computational Science, 2010. **5**(2): p. 149-197.
4. Balboa, F., et al., Staggered schemes for fluctuating hydrodynamics. Multiscale Modeling & Simulation, 2012. **10**(4): p. 1369-1408.
5. Donev, A., et al., *Low Mach number fluctuating hydrodynamics of diffusively mixing fluids.* Communications in Applied Mathematics and Computational Science, 2014. **9**(1): p. 47-105.
6. Naji, A., P.J. Atzberger, and F.L. Brown, Hybrid elastic and discrete-particle approach to biomembrane dynamics with application to the mobility of curved integral membrane proteins. Physical review letters, 2009. **102**(13): p. 138102.
7. Chinappi, M., et al., Molecular dynamics simulation of ratchet motion in an asymmetric nanochannel. Physical review letters, 2006. **97**(14): p. 144509.
8. Peskin, C.S., G.M. Odell, and G.F. Oster, Cellular motions and thermal fluctuations: the Brownian ratchet. Biophysical journal, 1993. **65**(1): p. 316-324.
9. Chow, C.C. and M.A. Buice, Path integral methods for stochastic differential equations. The Journal of Mathematical Neuroscience (JMN), 2015. **5**(1): p. 8.
10. Brennen, C.E., *Cavitation and bubble dynamics*. 2013: Cambridge University Press.
11. Cao, L., et al., Anti-icing superhydrophobic coatings. Langmuir, 2009. **25**(21): p. 12444-12448.

*Corresponding Author, Carlo Massimo Casciola: carlomassimo.casciola@uniroma1.it

12.Tinti, A., et al., *Intrusion and extrusion of water in hydrophobic nanopores.* Proceedings of the National Academy of Sciences, 2017: p. 201714796.
13.Jones, S., G. Evans, and K. Galvin, *Bubble nucleation from gas cavities—a review.* Advances in colloid and interface science, 1999. **80**(1): p. 27-50.
14.Kashchiev, D. and G. Van Rosmalen, *Nucleation in solutions revisited.* Crystal Research and Technology, 2003. **38**(7−8): p. 555-574.
15.Giacomello, A., et al., Geometry as a catalyst: how vapor cavities nucleate from defects. Langmuir, 2013. **29**(48): p. 14873-14884.
16.Amabili, M., et al., Wetting and cavitation pathways on nanodecorated surfaces. Soft matter, 2016. **12**(12): p. 3046-3055.
17.Lohse, D. and A. Prosperetti, Homogeneous nucleation: Patching the way from the macroscopic to the nanoscopic description. Proceedings of the National Academy of Sciences, 2016. **113**(48): p. 13549-13550.
18.Diemand, J., et al., Direct simulations of homogeneous bubble nucleation: Agreement with classical nucleation theory and no local hot spots. Physical review E, 2014. **90**(5): p. 052407.
19.Lutsko, J.F., Density functional theory of inhomogeneous liquids. IV. Squared-gradient approximation and classical nucleation theory. The Journal of chemical physics, 2011. **134**(16): p. 164501.
20.Gallo, M., F. Magaletti, and C.M. Casciola, *Fluctuating Hydrodynamics As A Tool To Investigate Nucleation Of Cavitation Bubbles.* International Journal of Computational Methods and Experimental Measurements, 2017. **6**(2): p. 345-357.
21.Magaletti, F., L. Marino, and C.M. Casciola, Shock Wave Formation in the Collapse of a Vapor Nanobubble. Physical Review Letters, 2015. **114**(6): p. 064501.
22.Magaletti, F., et al., Shock-induced collapse of a vapor nanobubble near solid boundaries. International Journal of Multiphase Flow, 2016. **84**: p. 34-45.
23.Chaudhri, A., et al., Modeling multiphase flow using fluctuating hydrodynamics. Physical Review E, 2014. **90**(3): p. 033014.
24.Johnson, J.K., J.A. Zollweg, and K.E. Gubbins, *The Lennard-Jones equation of state revisited.* Molecular Physics, 1993. **78**(3): p. 591-618.
25.Weinan, E., W. Ren, and E. Vanden-Eijnden, Simplified and improved string method for computing the minimum energy paths in barrier-crossing events. The Journal of chemical physics, 2007.
26.Giacomello, A., et al., Mechanism of the Cassie-Wenzel transition via the atomistic and continuum string methods. The Journal of chemical physics, 2015. **142**(10): p. 104701.
27.Blander, M. and J.L. Katz, *Bubble nucleation in liquids*. AIChE Journal, 1975. **21**(5): p. 833-848.
28.Dell'Isola, F., H. Gouin, and G. Rotoli, Nucleation of spherical shell-like interfaces by second gradient theory: numerical simulations. arXiv preprint arXiv:0906.1897, 2009.
29.Magaletti, F., et al., The sharp-interface limit of the Cahn–Hilliard/Navier–Stokes model for binary fluids. Journal of Fluid Mechanics, 2013. **714**: p. 95-126.

*Corresponding Author, Carlo Massimo Casciola: carlomassimo.casciola@uniroma1.it